Simplified thermal lattice Boltzmann model for incompressible thermal flows

Y. Peng, C. Shu, and Y. T. Chew
Department of Mechanical Engineering, National University of Singapore, 10 Kent Ridge Crescent, Singapore 119260
(Received 10 October 2002; revised manuscript received 31 March 2003; published 7 August 2003)

Considering the fact that the compression work done by the pressure and the viscous heat dissipation can be neglected for the incompressible flow, and its relationship with the gradient term in the evolution equation for the temperature in the thermal energy distribution model, a simplified thermal energy distribution model is proposed. This thermal model does not have any gradient term and is much easier to be implemented. This model is validated by the numerical simulation of the natural convection in a square cavity at a wide range of Rayleigh numbers. Numerical experiments showed that the simplified thermal model can keep the same order of accuracy as the thermal energy distribution model, but it requires much less computational effort.

DOI: 10.1103/PhysRevE.68.026701 PACS number(s): 45.50.−j, 47.11.+j

I. INTRODUCTION

The kinetic nature of the lattice Boltzmann method (LBM) has helped in developing it into an alternative method for fluid dynamics in the past ten years [1]. Although it has been successfully used in the isothermal flow problems, its application in the heat transfer system has not achieved such great success because of the severe numerical instability for the thermal models.

In general, the current thermal models fall into the following categories: the passive scalar approach, the multispeed approach, and the thermal energy distribution model proposed by He, Chen, and Doolen [2]. Previous work [2–4] showed that the thermal energy distribution model is a suitable tool for solving real thermal problems. But, there still exist some shortcomings for this thermal model. On one hand, it contains one complicated gradient operator term in the evolution equation for the temperature, and thus the simplicity property of the LBM has been lost. On the other hand, since the viscosity is involved not only in the momentum equation but also in the energy equation, the new variables for the thermal energy distribution functions are used so as to keep the viscosity consistent in the governing equations for the thermal energy distribution model and to avoid the implicitness of the scheme [2]. The governing equations are transformed to the forms whose variables are the new density distributions. However, the simple bounce-back condition for the nonequilibrium functions is the relationship for the old density distributions. Such relationship becomes very complicated after changing to the new forms for the new variables, since the evolution equations are for the new variables. This leads to the loss of one good feature for the LBM that boundary condition can be easily implemented. The detailed explanation of these drawbacks will be shown in the following section.

In this paper, a simplified thermal energy distribution model is proposed by us to overcome the above shortcomings. This simplified thermal model is based on the assumption that in real incompressible applications, the compression work done by the pressure and the viscous heat dissipation can be neglected. Our study found that the complicated gradient operator term in the original thermal energy distribution model is mainly used to recover the compression work and the viscous heat dissipation. So this term is intentionally discarded by us. After this simplification, there is no viscous term in the evolution equation for the new density distribution function, so there is no need to introduce the new variables to keep the viscosity same for both governing equations. As a result, the above-mentioned two shortcomings for the original thermal energy distribution model can be overcome.

Our simplified thermal model is validated by the numerical simulation of the natural convection in a square cavity at a wide range of Rayleigh numbers. Its improvement in the efficiency to get the same accurate results is demonstrated by the comparison with numerical results using the original thermal model. Its compressibility is also studied by the comparison with numerical results using the incompressible lattice Boltzmann Bhatnagar-Gross-Krook (LBGK) model in the simplified thermal energy distribution model.

II. SIMPLIFIED THERMAL ENERGY DISTRIBUTION MODEL

A. Original thermal energy distribution model

The thermal energy distribution model uses a new distribution function to simulate the temperature field. The macroscopic density and velocity fields are still simulated using the density distribution function.

The density distribution function and the new distribution function satisfy the following equations, respectively:

$$\bar{f}_\alpha(x+e_\alpha\delta t,t+\delta t)-\bar{f}_\alpha(x,t)=-\frac{\delta t}{\tau_\nu+1/2\delta t}[\bar{f}_\alpha(x,t)-f_\alpha^{\mathrm{eq}}(x,t)]+\frac{\tau_\nu F_\alpha\delta t}{\tau_\nu+1/2\delta t}, \tag{1}$$

$$\bar{g}_\alpha(x+e_\alpha\delta t,t+\delta t)-\bar{g}_\alpha(x,t)=-\frac{\delta t}{\tau_c+1/2\delta t}[\bar{g}_\alpha(x,t)-g_\alpha^{\mathrm{eq}}(x,t)]-\frac{\tau_c f_\alpha(x,t)q_\alpha\delta t}{\tau_c+1/2\delta t}, \tag{2}$$

where

$$\overline{f}_\alpha = f_\alpha + \frac{\delta t}{2\tau_\nu}(f_\alpha - f_\alpha^{\mathrm{eq}}) - \frac{\delta t}{2}F_\alpha, \tag{3a}$$

$$\overline{g}_\alpha = g_\alpha + \frac{\delta t}{2\tau_c}(g_\alpha - g_\alpha^{\mathrm{eq}}) + \frac{\delta t}{2}f_\alpha q_\alpha, \tag{3b}$$

$$F_\alpha = \frac{\vec{G}\cdot(\vec{e}_\alpha - \vec{V})}{RT} f_\alpha^{\mathrm{eq}}, \tag{3c}$$

$$q_\alpha = (\vec{e}_\alpha - \vec{V})\cdot\left[\frac{1}{\rho}(-\nabla p + \nabla\cdot\Pi) + (\vec{e}_\alpha - \vec{V})\cdot\nabla\vec{V}\right], \tag{3d}$$

$$\Pi = \rho\upsilon(\nabla\vec{V} + \vec{V}\nabla), \tag{3e}$$

and $\vec{G}$ are the external forces acting on the unit mass. It can be seen in Eq. (2) that there exists a complicated gradient term $f_\alpha q_\alpha$. The simplicity property of the LBM has been lost.

Two new variables $\overline{f}$, $\overline{g}$ for the thermal energy distribution model are used so as to keep the consistency of the viscosity and to keep the scheme explicit [2]. In the isothermal LBM, the evolution equation for the density distribution is

$$f_\alpha(x + e_\alpha\delta t, t+\delta t) - f_\alpha(x,t) = -\frac{1}{\tau_\nu}[f_\alpha(x,t) - f_\alpha^{\mathrm{eq}}(x,t)] + \delta t F_\alpha. \tag{4}$$

This introduces a second-order truncation error and this truncation error is fortunately nondestructive because it can be totally absorbed into the physical viscous term. The only effect is the change of the viscosity from $\upsilon = \tau_\nu c_5^2 \delta t$ to $\upsilon = (\tau_\nu - \frac{1}{2})c_5^2\delta t$. However, this will cause some problem for the thermal LBM, because the density distribution function exists in both equations. During the Chapman-Enskog multiscale expansions, its nonequilibrium part, which comes from the first-order Chapman-Enskog approximation and has nothing to do with the second-order Chapman-Enskog approximation, is used by the gradient term in Eq. (2) to recover the viscous heat dissipation term in the macroscopic energy equation. This means that the viscosity in the viscous heat dissipation term should be $\upsilon = \tau_\nu c_5^2\delta t$, which is inconsistent with the viscosity $\upsilon = (\tau_\nu - \frac{1}{2})c_5^2\delta t$ in Eq. (4). So the new variables and their governing equations have to be used.

It is worth to mention that the old variable f_α for the density distribution function is used for the expressions of $\overline{g}_\alpha$ and $\tau_c f_\alpha(x, e_\alpha, t) q_\alpha \delta t/(\tau_c + 1/2\delta t)$ in Eq. (2).

The bounce-back rule of the nonequilibrium distribution function proposed by Zou and He [5] is used for the boundary condition. The density distribution function at the boundary should satisfy the following condition:

$$f_\alpha^{\mathrm{neq}} = f_\beta^{\mathrm{neq}}, \tag{5}$$

where e_α and e_β have opposite directions. The new density distribution function at the boundary satisfies

$$g_\alpha^{\mathrm{neq}} - e_\alpha^2 f_\alpha^{\mathrm{neq}} = -(g_\beta^{\mathrm{neq}} - e_\beta^2 f_\beta^{\mathrm{neq}}). \tag{6}$$

It should be emphasized that the old variables of the thermal energy distribution model are used in the boundary condition, Eqs. (5) and (6), while the governing equations are for the new variables. Transformation is needed for every time step and the extra computational effort is introduced.

B. Simplified thermal energy distribution model

We can see from the above section that the use of the new variables is due to the requirement that the viscosity in the two governing equations for the thermal energy distribution model should be consistent. It is well accepted that the viscous heat dissipation term in the energy equation can be neglected for the incompressible flow. So, the omitting of the viscous heat dissipation and compression work done by pressure in macroscopic energy equation can be reflected by dropping out the gradient term in the evolution equation for the new distribution function, since such gradient term is mainly used to recover these terms through the Chapman-Enskog expansion. Based on this consideration, the simplified thermal energy distribution model is proposed.

The governing equations for the simplified thermal energy distribution model are

$$f_\alpha(x + e_\alpha\delta t, t+\delta t) - f_\alpha(x,t) = -\frac{1}{\tau_\nu}[f_\alpha(x,t) - f_\alpha^{\mathrm{eq}}(x,t)] + \delta t F_\alpha, \tag{7}$$

$$g_\alpha(x + e_\alpha\delta t, t+\delta t) - g_\alpha(x,t) = -\frac{1}{\tau_c}[g_\alpha(x,t) - g_\alpha^{\mathrm{eq}}(x,t)]. \tag{8}$$

When the 9-bit model, which is defined as

$$\vec{e}_\alpha = \begin{cases} 0, & \alpha = 0 \\ \{\cos[(\alpha-1)\pi/2], \sin[(\alpha-1)\pi/2]\}c, & \alpha = 1,2,3,4 \\ \sqrt{2}\{\cos[(\alpha-5)\pi/2 + \pi/4], \sin[(\alpha-5)\pi/2 + \pi/4]\}c, & \alpha = 5,6,7,8 \end{cases} \tag{9}$$

is used, the equilibrium function for the density distribution function is given as

$$f_\alpha^{\mathrm{eq}} = w_\alpha \rho\left[1 + \frac{3\vec{e}_\alpha\cdot\vec{V}}{c^2} + \frac{9(\vec{e}_\alpha\cdot\vec{V})^2}{2c^2} - \frac{3\vec{V}^2}{2c^2}\right], \tag{10}$$

where $w_0 = \frac{4}{9}$, $w_\alpha = \frac{1}{9}$ for $\alpha = 1,2,3,4$, $w_\alpha = \frac{1}{36}$ for $\alpha = 5,6,7,8$. Similarly, following the work of He, Chen, and Doolen [2], the equilibrium distribution functions for the new thermal energy distribution g can be written as

$$g_0^{\mathrm{eq}} = -\frac{2\rho\varepsilon}{3}\frac{\vec{V}^2}{c^2}, \tag{11a}$$

$$g_{1,2,3,4}^{\mathrm{eq}} = \frac{\rho\varepsilon}{9}\left[\frac{3}{2} + \frac{3}{2}\frac{\vec{e}_\alpha\cdot\vec{V}}{c^2} + \frac{9}{2}\frac{(\vec{e}_\alpha\cdot\vec{V})^2}{c^4} - \frac{3}{2}\frac{\vec{V}^2}{c^2}\right], \tag{11b}$$

$$g_{5,6,7,8}^{\mathrm{eq}} = \frac{\rho\varepsilon}{36}\left[3 + 6\frac{\vec{e}_\alpha\cdot\vec{V}}{c^2} + \frac{9}{2}\frac{(\vec{e}_\alpha\cdot\vec{V})^2}{c^4} - \frac{3}{2}\frac{\vec{V}^2}{c^2}\right], \tag{11c}$$

where $\varepsilon = DRT/2$. Then the macroscopic density, velocity, and temperature are calculated by

$$\rho = \sum_\alpha f_\alpha, \tag{12a}$$

$$\rho\vec{V} = \sum_\alpha \vec{e}_\alpha f_\alpha, \tag{12b}$$

$$\rho\varepsilon = \sum_\alpha g_\alpha. \tag{12c}$$

The Chapman-Enskog expansion for the density distribution function can recover the continuity and Navier-Stokes (NS) equation. The detailed derivation of this is given by Hou *et al.* [6] and will not be shown here. The viscosity is determined by

$$\upsilon = (\tau_\nu - \tfrac{1}{2})c_5^2\delta t. \tag{13}$$

It can be shown that the macroscopic energy equation can be derived from the evolution equation for the new thermal energy distribution function by the Chapman-Enskog expansion following the same procedure as Hou *et al.* [6]. The Taylor series expansion for Eq. (8) to $O(\delta^2)$ results in

$$\delta(\partial_t + \vec{e}\cdot\vec{\nabla})g_\alpha + \frac{\delta^2}{2}[\partial_t + \vec{e}\cdot\vec{\nabla}]^2 g_\alpha + O(\delta^2) = -\frac{1}{\tau_c}(g_\alpha - g_\alpha^{(0)}), \tag{14}$$

where g_α^{eq} is represented as $g_\alpha^{(0)}$. Expanding g_α about $g_\alpha^{(0)}$, we can get

$$g_\alpha = g_\alpha^{(0)} + \delta g_\alpha^{(1)} + \delta^2 g_\alpha^{(2)} + O(\delta^2). \tag{15}$$

The first-order expansion of Eq. (14) is

$$(\partial_{t0} + \vec{e}\cdot\vec{\nabla})g_\alpha^{(0)} = -\frac{1}{\tau_c}g_\alpha^{(1)}. \tag{16}$$

The second-order expansion of Eq. (14) is

$$\partial_{t1}g_\alpha^{(0)} + \left(1 - \frac{1}{2\tau_c}\right)(\partial_{t0} + \vec{e}\cdot\vec{\nabla})g_\alpha^{(1)} = -\frac{1}{\tau_c}g_\alpha^{(2)}. \tag{17}$$

Taking summation of Eqs. (16) and (17), we can get

$$\partial_{t0}(\rho\varepsilon) + \vec{\nabla}\cdot(\rho\vec{V}\varepsilon) = 0, \tag{18}$$

$$\partial_{t1}(\rho\varepsilon) + \left(1 - \frac{1}{2\tau_c}\right)\Pi^{(1)} = 0, \tag{19}$$

where $\Pi^{(1)} = \Sigma_\alpha(\partial_{t0} + \vec{e}\cdot\vec{\nabla})g_\alpha^{(1)}$ and it is $\Pi^{(1)} = -\tau_c\frac{2}{3}\nabla^2(\rho\varepsilon)$ after neglecting the terms of $O(u^2\delta T)$. Combining Eqs. (18) and (19), we can get

$$\partial_t(\rho\varepsilon) + \vec{\nabla}\cdot(\rho\vec{V}\varepsilon) = \chi\nabla^2(\rho\varepsilon). \tag{20}$$

The diffusivity χ is determined by

$$\chi = \tfrac{2}{3}(\tau_c - \tfrac{1}{2})c^2\delta t. \tag{21}$$

From the above derivation, we can see that evolution equations (7) and (8) can recover the macroscopic continuity, NS equation, and energy equation through the Chapman-Enskog expansion.

This simplified thermal energy distribution model has the following good features as compared with the original thermal energy distribution model. First, it does not include the complex gradient term in the evolution equation for the new density distribution function and keeps the same simple form as the isothermal LBM. Second, it does not use the new variables. This simplifies the calculation process. Third, the bounce-back rule of the nonequilibrium distribution function is also used for the boundary condition for this simplified thermal model. But it is very easy for the simplified model to implement, since the variables for the evolution equations and the boundary conditions are consistent.

C. The accuracy of the simplified thermal energy distribution model in space

Before we do the numerical simulation using the simplified thermal energy distribution model, we need to study its accuracy in space. We take the porous plate problem as a test case for the study, since it has the analytical solution. The problem is a channel flow where the upper cool plate moves with a constant velocity, and a constant normal flow of fluid is injected through the bottom warm plate and withdrawn at the same rate from the upper plate. The analytical solution of the velocity field in steady state is given by

$$u = u_0\left(\frac{e^{(\mathrm{Re}\,y/L)} - 1}{e^{\mathrm{Re}} - 1}\right), \tag{22}$$

where u_0 is the velocity of the upper plate, Re is the Reynolds number based on the inject velocity v_0, and the channel width is L. The temperature profile in the steady state satisfies

$$T = T_0 + \Delta T\left(\frac{e^{(\mathrm{Pr}\,\mathrm{Re}\,y/L)} - 1}{e^{\mathrm{Pr}\,\mathrm{Re}} - 1}\right), \tag{23}$$

where $\Delta T = T_1 - T_0$ is the temperature difference between the hot bottom plate with temperature T_1 and the cool wall

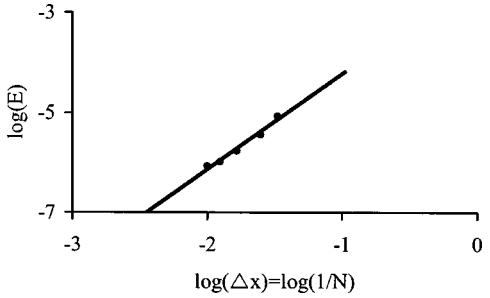

FIG. 1. Numerical error versus lattice spacing for the porous plate flow.

with temperature T_0. Another two dimensionless parameters are $\mathrm{Pr}=\nu/\chi$ and $\mathrm{Ra}=(g\beta\Delta TL^3)/(\nu\chi)$ (where Pr is the Prandtl number and Ra is the Rayleigh number).

Simulations were carried out to evaluate the numerical accuracy in space of the model. In the simulations, the Prandtl number is set to be 0.71, Re=10, and Ra=100. The lattice spacing Δx varies from $\frac{1}{30}$ to $\frac{1}{100}$. Relative global errors in temperature field were measured and defined by

$$E=\frac{\sqrt{\Sigma_{i,j}|T(x,y)-T_a(x,y)|^2}}{\sqrt{\Sigma_{i,j}|T_a(x,y)|^2}}, \tag{24}$$

where the summation is over the entire field and T_a is the analytical solution. Suppose that the order of accuracy of the model is n. Then we have the following relationship:

$$E=C(\Delta x)^n, \tag{25}$$

where C is a constant. Equation (25) can also be written as

$$\ln(E)=\ln(C)+n\ln(\Delta x). \tag{26}$$

Clearly, $\ln(E)$ has a linear relationship with $\ln(\Delta x)$. This is confirmed by Fig. 1, which shows $\ln(E)$ versus $\ln(\Delta x)$. The fitting curve is a straight line whose slope is n. From Fig. 1, we obtain $n=2.02$. This implies that the present model is of second order in space. The velocity and temperature profiles for this case are shown in Fig. 2. They agree very well with the analytical solutions.

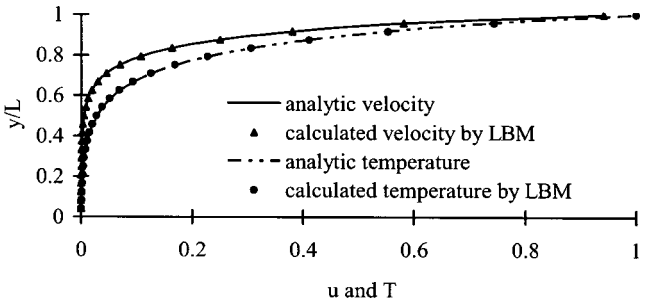

FIG. 2. Velocity and temperature profiles in the porous plate flow.

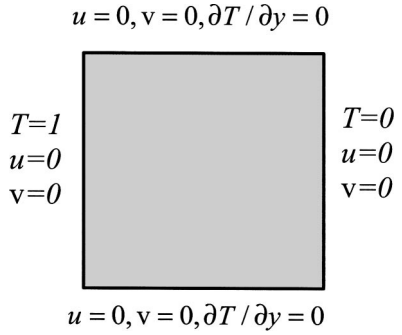

FIG. 3. Configuration of natural convection in a square cavity.

III. NUMERICAL SIMULATION OF NATURAL CONVECTION IN A SQUARE CAVITY

In order to validate the simplified thermal energy distribution model, we carried out the computation for a sample problem. The problem considered is a natural convection in a two-dimensional square cavity with sidewalls maintained at different temperatures. The temperature difference between the walls introduces a temperature gradient in the fluid, and the consequent density difference induces a fluid motion, that is, convection. The top and bottom walls are adiabatic. The problem definition and the boundary conditions are displayed in Fig. 3.

A. Dimensionless parameters and relaxation times

The Boussinesq approximation is applied to the buoyancy force term. This means that the properties β and ν are considered as constants, and the buoyancy term is assumed to depend linearly on the temperature,

$$\rho\vec{G}=\rho\beta g_0(T-T_m)\vec{j}, \tag{27}$$

where β is the thermal expansion coefficient, g_0 is the acceleration due to gravity, T_m is the average temperature, and $\vec{j}$ is the vertical direction opposite to that of gravity.

The dynamical similarity depends on two dimensionless parameters: the Prandtl number Pr and the Rayleigh number Ra,

$$\mathrm{Pr}=\nu/\chi, \quad \mathrm{Ra}=(\beta g_0\Delta TH^3)/(\nu\chi). \tag{28}$$

To ensure that the code is working properly in the near-incompressible regime, we carefully choose the value of $\beta g_0\Delta TH$. Once $\beta g_0\Delta TH$ is determined, the kinetic viscosity and the thermal diffusivity are determined through the two dimensionless numbers Pr and Ra. By using Eqs. (13) and (21), two relaxation times τ_ν,τ_c are determined. The Nusselt number Nu is one of the most important dimensionless parameters in describing the convective heat transport. Its average in the whole flow domain is defined by

$$\overline{\mathrm{Nu}}=\frac{H}{\chi\Delta T}\frac{1}{H^2}\int_0^H\int_0^H q_x(x,y)\,dx\,dy, \tag{29}$$

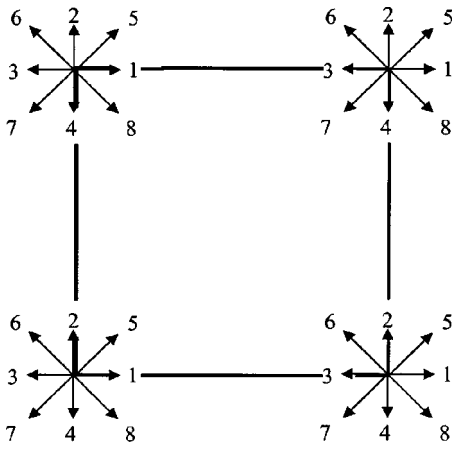

FIG. 4. Schematic plot of velocity directions at four corner points.

where $q_x(x,y)=uT(x,y)-\chi(\partial/\partial x)T(x,y)$ is the local heat flux in horizontal direction.

B. Implementation of the boundary condition

The bounce-back rule of the nonequilibrium distribution function is used in this work. At four corner points, the different treatment at some special particle directions is needed. The schematic plot of velocity directions of the 9-bit model at four corner points is shown in Fig. 4. At the particle directions 6 and 8 for the left bottom and right upper corner points, the particle directions 5 and 7 for the left upper and right bottom corner points, their values for the thermal energy distribution functions cannot be determined from their evolution equations and the bounce-back boundary condition. Since these values do not transport any information into the interior points, the equilibrium functions are given for the two distribution functions. For the adiabatic boundary condition, the temperature on the wall is unknown. In order to use the above-mentioned bounce-back condition, we transfer it to the Dirichlet-type condition by using the conventional second-order finite difference approximation to get the temperature on the boundary [4].

C. Grid and convergence criterion

The uniform grid is used for all of the following numerical simulations.

The convergence criterion for all the cases is set to

$$\max[|\sqrt{(u^{n+1})^2+(v^{n+1})^2}-\sqrt{(u^n)^2+(v^n)^2}|]\leqslant 10^{-8},$$

$$\max|T^{n+1}-T^n|\leqslant 10^{-8}, \tag{30}$$

where n and $n+1$ represent the old and new time levels, respectively.

All the calculation is done on the PC PIV-1.6G.

IV. RESULTS AND DISCUSSION

A. Validation of the numerical results and analysis of flow and thermal fields

Table I shows the numerical results of the maximum horizontal velocity on the vertical midplane of the cavity, $u_{\max}$, and its location Y, the maximum vertical velocity on the horizontal midplane of the cavity, $v_{\max}$, and its location X, the average Nusselt number throughout the cavity $\overline{\mathrm{Nu}}$ for a wide range of Rayleigh numbers using the simplified thermal energy distribution model. The numerical results of Navier-Stokes equations given by Shu and Xue [7] using the differential quadrature (DQ) method are also included for comparison. Note that the velocity shown in the table is

TABLE I. Comparison of numerical results among the simplified thermal energy distribution model, original thermal energy distribution model, and a Navier-Stokes solver.

Ra		10^3	10^4	10^5	10^6
$u_{\max}$	Simplified	3.644	16.134	34.261	63.024
	Original	3.649	16.156	34.245	63.527
	DQ [7]	3.649	16.190	34.736	64.775
y	Simplified	0.810	0.820	0.855	0.848
	Original	0.810	0.820	0.855	0.844
	DQ [7]	0.815	0.825	0.855	0.850
$v_{\max}$	Simplified	3.691	19.552	67.799	215.26
	Original	3.700	19.679	68.276	218.47
	DQ [7]	3.698	19.638	68.640	220.64
x	Simplified	0.180	0.120	0.065	0.040
	Original	0.180	0.120	0.065	0.040
	DQ [7]	0.180	0.120	0.065	0.035
$\overline{\mathrm{Nu}}$	Simplified	1.117	2.241	4.511	8.731
	Original	1.117	2.244	4.520	8.781
	DQ [7]	1.118	2.245	4.523	8.762
CPU (s)	Simplified	1386.0	7010.7	35 666.0	98 617.3
	Original	2297.0	17 864.7	96 296.6	171 659.3

TABLE II. Grid-dependence study for the natural convection in a square cavity at $\mathrm{Ra}=10^4$.

Mesh	51×51	101×101	151×151	201×201	DQ
$u_{\max}$	16.082	16.128	16.134	16.155	16.190
y	0.820	0.820	0.820	0.825	0.825
$v_{\max}$	19.451	19.504	19.552	19.666	19.638
x	0.120	0.120	0.120	0.120	0.120
$\overline{\mathrm{Nu}}$	2.210	2.232	2.241	2.242	2.245

normalized by the reference velocity of χ/H, where χ is the thermal diffusivity and H is the height of the square cavity.

The grid-dependence study of the results is examined before the comparison. One example of the Rayleigh number of 10^4 is given in Table II. In this study, the number of grid points is taken the same in both the x and y directions. That is, the grid size is taken as $N\times N$, where N is the grid number in each spatial direction. The calculated average Nusselt number changing with N is shown in Table II. From this table, we can clearly see that when N increases, the calculated average Nusselt number quickly approaches the benchmark result. When N further increases from 151 to 201, there is not much improvement for the result. So we can say that for $\mathrm{Ra}=10^4$, the grid size of 151×151 can give very accurate results. The relative errors for the average Nusselt number defined by

$$E=\frac{\sqrt{(\overline{\mathrm{Nu}}-\overline{\mathrm{Nu}_a})^2}}{\sqrt{\overline{\mathrm{Nu}_a^2}}}, \tag{31}$$

where $\overline{\mathrm{Nu}}_a$ is the benchmark solution, versus lattice spacing are shown in Fig. 5. From this figure, we can see that the slope of the fitting line is 1.96. This confirms that the present model is around second order in space. Through the grid-dependence study, the grid sizes of 101×101 for $\mathrm{Ra}=10^3$, 151×151 for $\mathrm{Ra}=10^4$, 201×201 for $\mathrm{Ra}=10^5$, and 251×251 for $\mathrm{Ra}=10^6$ are found to be sufficient for engineering purposes. So the above comparisons are done on those grids.

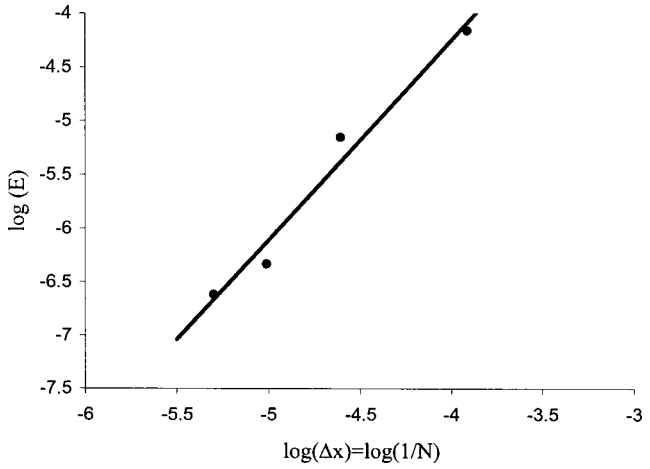

FIG. 5. Numerical errors for the average Nusselt number versus lattice spacing for the natural convection at $\mathrm{Ra}=10^4$.

From Table I, we can see that the numerical results using the simplified thermal energy distribution model generally agree well with the benchmark results of Shu and Xue [7] in a wide range of Rayleigh numbers. The deviation of the two results at high Rayleigh number is larger than that at low Rayleigh number. But these deviations are acceptable. So we can say that the present results are very accurate, and the present method can be used to solve the thermal problems accurately and effectively.

It can be seen from Table I that, with the increase of the Rayleigh number, due to the enhancement of natural convection, $u_{\max}$, $v_{\max}$, $\overline{\mathrm{Nu}}$ are increased greatly, and the position of maximum vertical velocity on the horizontal midplane moves closer to the wall. It is also found that the Nusselt number obtained by the present method is slightly smaller than the Navier-Stokes result of Shu and Xue [7], which agrees well with the phenomenon observed in the simulation of the Rayleigh-Benard convection by He, Chen, and Doolen [8]. Figures 6 and 7 show the streamlines and isotherms of $\mathrm{Ra}=10^3$, 10^4, 10^5, 10^6. These plots agree well with those obtained by Shu and Xue [7].

B. Comparison of our numerical results with those using the original thermal energy distribution model

In order to test the accuracy and efficiency of the simplified thermal energy distribution model as compared with the

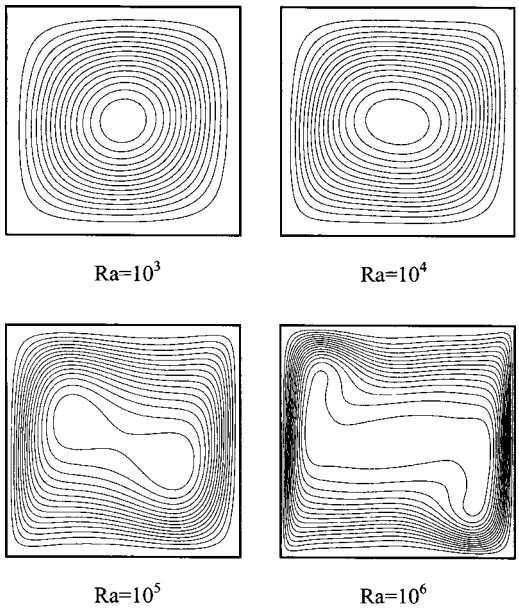

FIG. 6. Streamlines of $\mathrm{Ra}=10^3$, 10^4, 10^5, and 10^6.

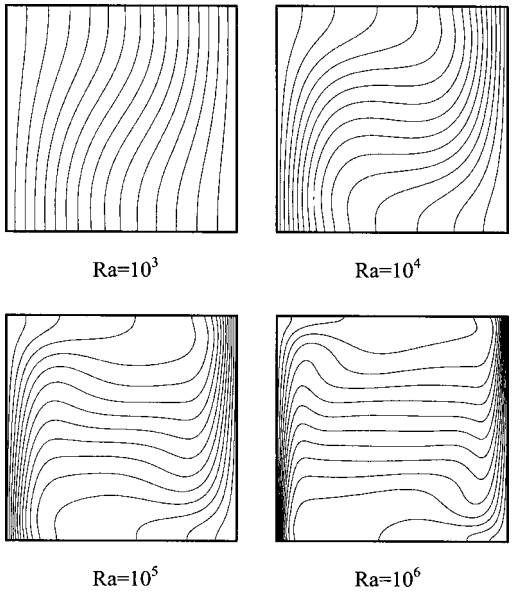

FIG. 7. Isotherms of $\mathrm{Ra}=10^3$, 10^4, 10^5, and 10^6.

original thermal energy distribution model, the numerical simulations for the same Rayleigh number on the same grid using the original thermal model are also carried out. These numerical results for the Rayleigh numbers of 10^3, 10^4, 10^5, and 10^6 are also given in Table I.

It can be observed from Table I that, for the same Rayleigh number and the same number of grid points, the calculated results using the simplified thermal model are almost the same as those using the original thermal model. This confirms our findings that the compression work done by the pressure and viscous heat dissipation term can be neglected for such incompressible flow, which leads to the omission of the gradient term in the original evolution equation for the new distribution function. So we can say that the simplified thermal model can get the same accurate results as the original thermal model.

As far as the computational efficiency is concerned, for the same grid size, the calculation time using the simplified thermal model is much less than that using the original thermal model. From Table I, we can see that for $\mathrm{Ra}=10^3$, the calculation time using the simplified thermal model is 1386.0 s, while the original thermal model takes 2297.0 s to get the converged solution. Similarly, for $\mathrm{Ra}=10^4-10^6$, only half or even less than half of the calculation time is needed for the simplified thermal model to get the converged results as compared with the original thermal model under the same Rayleigh number. This shows that our simplified thermal model is more efficient than the original thermal model at getting the same accurate results.

C. Compressibility study of the simplified thermal energy distribution model

In order to study the compressibility property of this scheme, we use an incompressible isothermal LBGK model proposed by Guo [9] to modify the evolution equation for the density distribution function in our simplified thermal energy distribution model. It should be pointed out that this incompressible scheme is, in fact, equivalent to the model previously proposed by He and Luo [10].

The density distribution function is changed into

$$f_\alpha(x+e_\alpha\delta t,t+\delta t)-f_\alpha(x,t)=-\frac{1}{\tau_\nu}[f_\alpha(x,t)-f_\alpha^{\mathrm{eq}}(x,t)]+F_\alpha, \tag{32}$$

where $F_\alpha=-\frac{1}{2}\delta t(\delta_{\alpha 2}+\delta_{\alpha 4})\vec{e}_\alpha\cdot\vec{j}g\beta(T-T_m)$,

$$f_\alpha^{\mathrm{eq}}=\begin{cases}-4\sigma p+s_0(\vec{V}), & \alpha=0\\ \lambda p+s_\alpha(\vec{V}), & \alpha=1,2,3,4\\ \gamma p+s_\alpha(\vec{V}), & \alpha=5,6,7,8,\end{cases}$$

$$s_\alpha(\vec{V})=w_\alpha\left[\frac{3\vec{e}_\alpha\cdot\vec{V}}{c^2}+\frac{9(\vec{e}_\alpha\cdot\vec{V})^2}{2c^2}-\frac{3\vec{V}^2}{2c^2}\right],$$

$$\sigma=\tfrac{5}{12},\quad \lambda=\tfrac{1}{3},\quad \gamma=\tfrac{1}{12}.$$

The macroscopic variables are calculated by

$$\vec{V}=\sum_{\alpha=1}^{8}e_\alpha f_\alpha,\quad p=\frac{1}{4\sigma}\left[\sum_{\alpha=1}^{8}f_\alpha+s_0(\vec{V})\right]. \tag{33}$$

Since this is a completely incompressible LBGK model, the Chapman-Enskog expansion of this evolution equation will recover the incompressible continuity and NS equation correctly. We compare the numerical results of natural convection in a square cavity for a wide range of Rayleigh numbers, using the incompressible LBGK model and without using the incompressible LBGK model to see the effect of the compressibility of our simplified thermal model.

Table III shows the numerical results of the maximum horizontal velocity on the vertical midplane of the cavity, $u_{\max}$, and its location Y, the maximum vertical velocity on the horizontal midplane of the cavity, $v_{\max}$, and its location X, the average Nusselt number throughout the cavity $\overline{\mathrm{Nu}}$ using the simplified thermal model with and without the incompressible LBGK model. The numerical results of Navier-Stokes equations given by Shu and Xue [7] using the DQ method are also included as benchmark data.

From Table III, we can see that the difference in the results using and without using the incompressible LBGK model is very small. But the results of the velocities using the incompressible LBGK model agree a little bit better with the benchmark results than those without using the incompressible model. The higher the Rayleigh number is, the better this improvement is. For example, for $\mathrm{Ra}=10^4$, the result of the maximum horizontal velocity on the vertical midplane of the cavity is 16.134 without using the incompressible model and 16.146 using the incompressible model, while the benchmark result is 16.190. This shows that there is a little bit of improvement for the maximum horizontal velocity on the vertical midplane if using the incompressible model. For a high Rayleigh number of 10^6, the maximum horizontal ve-

TABLE III. Comparison of results using and without using the incompressible LBGK model.

Ra		10^3	10^4	10^5	10^6
Grid		101×101	151×151	201×210	251×251
u_{max}	Using	3.650	16.146	34.315	63.671
	Without	3.644	16.134	34.261	63.024
	DQ [7]	3.649	16.190	34.736	64.775
y	Using	0.810	0.820	0.855	0.852
	Without	0.810	0.820	0.855	0.848
	DQ [7]	0.815	0.825	0.855	0.850
v_{max}	Using	3.704	19.593	68.012	217.57
	Without	3.691	19.552	67.799	215.26
	DQ [7]	3.698	19.638	68.640	220.64
x	Using	0.180	0.120	0.065	0.040
	Without	0.180	0.120	0.065	0.040
	DQ [7]	0.180	0.120	0.065	0.035
$\overline{\mathrm{Nu}}$	Using	1.117	2.241	4.508	8.737
	Without	1.117	2.241	4.511	8.731
	DQ [7]	1.118	2.245	4.523	8.762

locity on the vertical midplane of the cavity changes from 63.024 without using the incompressible model to 63.671 using the incompressible model, while the benchmark result is 64.775. The improvement is more obvious than that at a low Rayleigh number of 10^4. The same trend is applied to the maximum vertical velocity on the horizontal midplane of the cavity. There is not much change in the average Nusselt number. This is in line with the physical background of the incompressible LBGK model. Since the use of the incompressible LBGK model is only for the evolution equation of the density distribution function, which is used to calculate the pressure and velocity, the improvement for the velocities is straightforward, while for the evolution equation of the new distribution function we still need to introduce the assumption that the characteristic velocity $\sqrt{\beta g_0 \Delta T H}$ is within the incompressible limit. So there should not be much difference for the Nusselt number using or without using the incompressible LBGK model.

To sum up, this study shows that the compressibility effect of the simplified thermal model is very small and can be used to solve the incompressible thermal flow without introducing any incompressible LBGK model.

V. CONCLUSIONS

The numerical results of the natural convection in a square cavity for a wide range of Rayleigh numbers show that our simplified thermal energy distribution model can get the same accurate results more efficiently as the original thermal energy distribution model. The compressibility of this scheme is also studied and the results show that the compressibility effect of this scheme can be neglected. The simplification for the original thermal model agrees well with the physical explanation that the compression work done by the pressure and the viscous heat dissipation can be ignored for the incompressible flow. This scheme has the following good features. It does not include any gradient term in the evolution equations and it preserves the simplicity of the LBM. It is easier to implement as compared with the original thermal model. It is worth mentioning that although all the calculations are done on the uniform grid, its extension to the arbitrary mesh grid is straightforward by using the Taylor series expansion- and least-squares-based LBM (TLLBM). The use of TLLBM in the thermal model has been studied by Shu, Peng, and Chew [4].

[1] S. Chen and G. D. Doolen, Annu. Rev. Fluid Mech. **30**, 329 (1998).
[2] X. He, S. Chen, and G. D. Doolen, J. Comput. Phys. **146**, 282 (1998).
[3] J. Onishi, Y. Chen, and H. Ohashi, JSME Int. J., Ser. B **44**, 53 (2001).
[4] C. Shu, Y. Peng, and Y. T. Chew, Int. J. Mod. Phy. C **13**, 1399 (2002).
[5] Q. Zou and X. He, Phys. Fluids **9**, 1591 (1997).
[6] S. Hou, Q. Zou, S. Chen, G. Doolen, and A. C. Cogley, J. Comput. Phys. **118**, 329 (1995).
[7] C. Shu and H. Xue, Int. J. Heat Fluid Flow **19**, 59 (1998).
[8] X. He, S. Chen, and G. D. Doolen, J. Comput. Phys. **146**, 282 (1998).
[9] Z. Guo, B. Shi, and N. Wang, J. Comput. Phys. **165**, 288 (2000).
[10] X. He and L.-S. Luo, J. Stat. Phys. **88**, 927 (1997).